Reflection and Transmission of Equatorial Rossby Waves*

MICHAEL A. SPALL AND JOSEPH PEDLOSKY

Department of Physical Oceanography, Woods Hole Oceanographic Institution, Woods Hole, Massachusetts

(Manuscript received 16 February 2004, in final form 24 June 2004)

ABSTRACT

The interaction of equatorial Rossby waves with a western boundary perforated with one or more narrow gaps is investigated using a shallow-water numerical model and supporting theory. It is found that very little of the incident energy flux is reflected into eastward-propagating equatorial Kelvin waves provided that at least one gap is located within approximately a deformation radius of the equator. Because of the circulation theorem around an island, the existence of a second gap off the equator reduces the reflection of short Rossby waves and enhances the transmission of the incident energy into the western basin. The westward energy transmitted past the easternmost island is further reduced upon encountering islands to the west, even if these islands are located entirely within the "shadow" of the easternmost island. A localized patch of wind forcing was also used to generate low-frequency Rossby waves for cases with island configurations representative of the western equatorial Pacific. For both idealized islands and a coastline based on the 200-m isobath, the amount of incident energy reflected into Kelvin waves depends on both the duration of the wind event and the meridional decay scale of the anomalous winds. For wind events of 2-yr duration with a meridional decay scale of 700 km, the reflected energy is 37% of the incident flux, and the energy transmitted into the Indian Ocean is approximately 10% of the incident flux, very close to that predicted by previous theories. For shorter wind events or winds confined more closely to the equator the reflected energy is significantly less.

1. Introduction

The reflection of westward-propagating equatorial Rossby waves into eastward-propagating Kelvin waves has been proposed as an important feedback mechanism in the delayed oscillator models of the El Niño–Southern Oscillation (ENSO) variability in the Pacific Ocean (Schopf and Suarez 1988, Battisti 1988). The thickness anomaly of the eastward-propagating Kelvin wave counteracts the positive feedback between the upper ocean and atmosphere in the interior of the basin, thus providing an important negative feedback mechanism for sustaining the low-frequency oscillation. However, it has also been suggested that a southward shift in the wind anomalies may provide the forcing to trigger eastward-propagating Kelvin waves that result in the decay of ENSO events (Harrison and Vecchi 1999). The relative influences of reflection and local and remote forcing for wave generation in ENSO are not clear.

Clarke (1983) showed that 50% of the energy flux in a low-frequency mode-1 Rossby wave incident on a solid western boundary will reflect into an eastward-propagating Kelvin wave. The observed oceanic variability is difficult to decompose cleanly into incident Rossby waves and reflected and forced Kelvin waves, and analysis of Ocean Topography Experiment (TOPEX)/Poseidon data leads to sometimes conflicting conclusions. Previous studies have described the relative efficiency of wave reflection in terms of the reflected energy, reflected energy relative to that for a solid western boundary, and the reflected amplitude. For consistency, we report the reflection and transmission of energy as a percentage of the incident energy flux throughout this study. Boulanger et al. (2003) conclude that the reflection efficiency of Rossby waves at the western boundary of the Pacific is 40%–45% of the incident energy flux. Zang et al. (2002) find an upper bound for the reflection of 30% and conclude that reflected Rossby waves are unlikely to account for a significant amount of the Kelvin wave energy found in the interior of the equatorial Pacific Ocean. This latter study is consistent with the modeling study by Verschell et al. (1995) in which they find only weak Kelvin wave reflection for both wind-forced and Rossby wave pulse calculations. Li and Clarke (1994) find good correlation between sea surface height anomalies in the eastern and western Pacific, consistent with eastward Kelvin

* Woods Hole Oceanographic Institution Contribution Number 11114.

Corresponding author address: Dr. Michael A. Spall, Woods Hole Oceanographic Institution, WHOI MS #21, 360 Woods Hole Road, Woods Hole, MA 02543.
E-mail: mspall@whoi.edu

wave propagation along the equator and nonzero Kelvin wave reflection. However, as discussed by Harrison and Vecchi (1999), the existence of Kelvin waves in the mid-Pacific may not be due to wave reflection from the western Pacific, but instead be a result of a southward shift in the wind stress that arises in this phase of the ENSO cycle.

Important theoretical studies by Clarke (1991, hereinafter C91) and Du Penhoat and Cane (1991, hereinafter DuPC) suggest that the western boundary of the Pacific acts much like a solid boundary for the reflection problem. For idealized, but realistic, island configurations each of these studies produces reflections of approximately 35% of the incident energy flux. These analytic approaches require several assumptions regarding the dynamics of the governing equations and the geometry of the islands composing the Indonesian Throughflow. While each of these assumptions appear reasonable, it is not clear how they affect the amount of incident energy reflected into Kelvin waves. Previous modeling studies by Verschell et al. (1995) and Potemra (2001) have looked at the interaction of low frequency Rossby waves with the western Pacific boundary, but they did not discuss the wave reflection problem for a gappy boundary or explicitly calculate the reflected energy in their calculations.

There has also been work done for Rossby wave reflection and transmission at midlatitudes. The study by McKee (1972) shows that for a single narrow gap in a western boundary there will be very little energy transmitted through the gap. However, the introduction of a second gap drastically changes the problem. The existence of an island between the two basins (the two-gap problem) introduces an additional constraint, namely that a circulation integral around the island must be satisfied (Pedlosky and Spall 1999; Pedlosky 2000). For certain modes of variability, this results in very efficient transmission of energy from the eastern side of the island, through the gaps, and into the western basin.

Many aspects of wave reflection in the western Pacific, and their role in ENSO, remain not well understood. We focus most of our attention on the basic issue of how equatorial waves interact with a western boundary with one or more gaps near the equator. We consider cases of a single gap in the western boundary, two gaps (one island), and shadowed islands. Last, the reflection and transmission of Rossby waves generated by a patch of wind forcing in the middle of the Pacific Ocean are calculated for both an idealized representation of the Indonesian Throughflow and a case with coastlines based on the actual 200-m isobath.

2. The shallow-water model

The model used for this study solves the shallow-water equations, written in dimensional form as

$$\mathbf{v}_t + \mathbf{v}\cdot\nabla\mathbf{v} + \beta y\mathbf{k}\times\mathbf{v} = -g'\nabla h + A_v\nabla^2\mathbf{v} \quad \text{and} \quad (1)$$

$$h_t + \nabla\cdot(\mathbf{v}h) = A_h\nabla^2\mathbf{h}, \quad (2)$$

where $\mathbf{v} = u\mathbf{i} + v\mathbf{j}$ is the two-dimensional velocity vector, h is the layer thickness, g' is the reduced gravity, $\beta = 2\times10^{-13}$ cm^{-1} s^{-1} is the meridional gradient of the Coriolis parameter, y is meridional distance from the equator, and A_v and A_h are coefficients of lateral viscosity and thickness diffusivity (200 m^2 s^{-1}). The model is solved using second-order centered finite differences on a staggered C grid and third-order Adams–Bashforth time stepping. The lateral boundary conditions are no-slip and no-normal flow.

The resting layer thickness is 500 m and the reduced gravity $g' = 1$ cm s^{-2}. The equatorial deformation radius for the standard stratification and layer thickness is 334 km with a Kelvin wave speed of $c = 2.2$ m s^{-1}. For all idealized calculations the model grid spacing is 25 km, while for the calculation using the 200-m isobath as the coastline the grid spacing is 16.7 km. For the calculations in this section, the model is initialized with a layer thickness anomaly of a specified zonal wavelength and either a meridional mode-1 or mode-2 Rossby wave structure [see the appendix Eqs. (A1) and (A2) for details]. The model is integrated forward in time with no external forcing.

a. Examples with a single gap

An example of a Rossby wave incident on a western boundary with a single narrow gap of width 75 km located on the equator is shown in Fig. 1. The frequency of the Rossby wave is 5×10^{-7} s^{-1}, giving a period of 145 days and a wavelength $\lambda = 9224$ km. A single wavelength is initialized in the eastern basin centered at $x =$ 21 500 km with amplitude bounded by $h = \pm1$ m (Fig. 1a). (An animation of this calculation can be found online at http://www.whoi.edu/science/PO/people/mspall/eqwaves.html)

After 90 days (Fig. 1b), the wave has propagated to the west and is beginning to penetrate into the western basin. Remarkably, the nearly solid barrier offers little resistance to the westward propagation of the wave. The negative thickness anomaly of the wave penetrates into the western basin through the narrow gap and begins to propagate poleward in the form of boundary Kelvin waves along the western side of the barrier. These Kelvin waves then radiate their energy westward into the interior. Most of the energy takes the form of the first-mode Rossby wave, which continues to propagate to the west, away from the barrier. There is also evidence of short Rossby waves being reflected along the eastern side of the barrier. The original wave is slightly dispersive, leaving a weak negative anomaly in the initial wave position. There is no evidence of a Kelvin wave propagating eastward along the equator.

By day 250, the Rossby wave signal has propagated well into the western basin. The first-mode meridional structure is reconstituted after the thickness anomalies

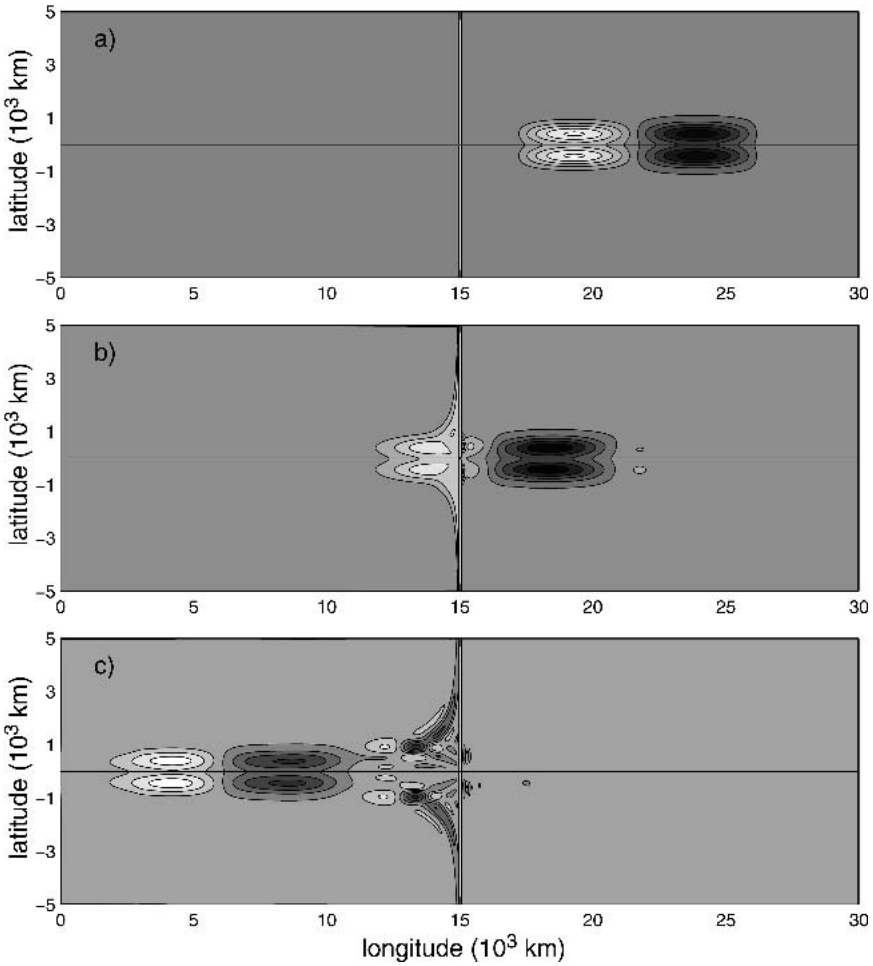

FIG. 1. Layer thickness anomaly for a first-mode Rossby wave of frequency 5×10^{-7} s^{-1} and a single gap of width 75 km located on the equator on days (a) 0, (b) 90, and (c) 250.

have propagated through the narrow gap. The amplitude of the wave is less than it was originally, but it still remains significant. There is also considerable energy in the western basin of smaller zonal and meridional scale that remains trapped to the eastern boundary.

Short reflected mode-1 Rossby waves are evident on the eastern side of the barrier. There is still no evidence of a reflected Kelvin wave in the eastern basin. The lack of reflected Kelvin waves for the case of a very narrow gap on the equator is consistent with the theory of Du Penhoat and Cane (1991). However, we find here that the Rossby wave re-forms on the western side of the barrier, while their theory, which assumes zero frequency, predicts two narrow jets extending from the poleward limits of the gap. The theory, outlined in the appendix, produces a very similar signal west of a delta function gap; long propagating mode-1 Rossby waves and trapped modes with smaller scales (not shown). Approximately 58% of the incident energy continues to propagate westward in the western basin. This is in stark contrast to the midlatitude problem in which very little of the incident energy flux is able to penetrate through a single narrow gap (McKee 1972).

We performed a simple experiment in which a Kelvin wave was initialized in the western basin and allowed to propagate toward a single, narrow gap located on the equator. Figure 2 shows the evolution of the interaction, and the principal result is clear. The Kelvin mode passes directly through the narrow gap and emerges, largely unaffected, to continue its eastward propagation. Approximately 77% of the incident energy flux from the western basin continues into the eastern basin. (An animation of this calculation can be found online at http://www.whoi.edu/science/PO/people/mspall/eqwaves.html)

We have come to understand this result in terms of the unique character of the Kelvin wave. Its meridional structure is completely determined by the double condition of zero potential vorticity and geostrophic balance for the zonal velocity. Once the height field at the equator is known, the complete meridional structure of the Kelvin wave is thus fixed. At the same time, the

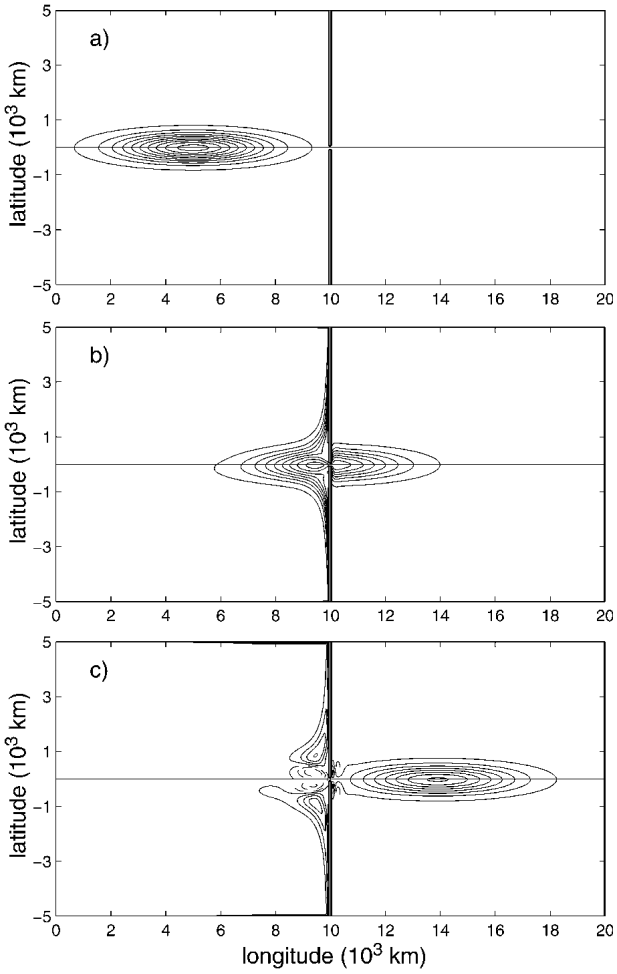

FIG. 2. Layer thickness for a Kelvin wave initialized in a western basin separated from the eastern basin by a single gap of width 125 km on days (a) 0, (b) 28, and (c) 50.

propagation equation for the height field at any latitude, in particular at the equator, is just the one-dimensional wave equation in x and t for the amplitude on the equator. With the open slot on the equator, the solution of that equation would yield an amplitude passing undisturbed through the slot from west to east and the spatial structure of the Kelvin wave, constrained by the zero potential vorticity condition, would be reconstituted on the eastern side of the boundary. This heuristic argument is consistent with our result in Fig. 2.

The consequences for the problem of Rossby waves impinging on the same barrier from the east are profound. The reflected waves, in general, consist of a set of short Rossby waves with eastward group velocities and, in the case of a mode-1 Rossby wave, an eastward-propagating Kelvin wave. However, we argue that the result of the Kelvin wave experiment in Fig. 2 suggests that for the reflection problem with an equatorial gap the reflected waves cannot contain the Kelvin mode since the radiation condition requires that none of the reflected wave energy come from the western basin.

Returning to the mode-1 Rossby wave, the amount of energy reflected into eastward-propagating Kelvin waves, normalized by the incident energy flux, has been calculated for a series of numerical integrations in which the location of the gap in the western boundary is shifted northward a distance δ (Fig. 3). The width of the gap in all of these cases is 75 km. The energy flux is calculated as $E(x) = \int_0^T \int_{-Y}^{Y} uh \, dy \, dt$, where T is the time of the integration and Y is the meridional extent of the basin. For the single gap problem, the energy flux is taken at $x = 10\,000$ km, which is westward of the trapped modes and represents that energy that is able to continue propagating to the west. In each of these cases, a sponge layer has been added to the westernmost 3000 km of the basin in which the thickness anomaly is restored toward zero with a time scale of 30 days. This inhibits the reflection of Kelvin waves from the western boundary so that there is no contamination of the energy flux near the barrier. The results show that the Kelvin wave reflection is very ineffective provided that the gap is located within a deformation radius of the equator. This result is similar to that predicted by Du Penhoat and Cane (1991), although we find generally less reflection into Kelvin waves (e.g., at $\delta/L_d = 1$ we find 15% energy reflection as compared with 30% for Du Penhoat and Cane).

In the previous example, the Rossby wave frequency $\omega/\omega_{\max} = 0.256$ is not particularly small, while the theory of Du Penhoat and Cane (1991) assumes $\omega/\omega_{\max} \ll 1$. We tested the sensitivity of the energy transmission into propagating modes in the western basin to the frequency of the incident Rossby wave. The maximum frequency of the mode-1 Rossby wave with a deformation radius of 334 km is $\omega_{\max} = 1.96 \times 10^{-6}\ \mathrm{s}^{-1}$ (period of 37 days). We carried out a series of calculations for which the period was varied between 42 days and 580 days ($\omega/\omega_{\max}$ ranging between 0.88 and 0.06). For the lowest two frequencies tested, the model domain was extended to 60 000 km in zonal extent and the model was initialized with only one-half wavelength of the ini-

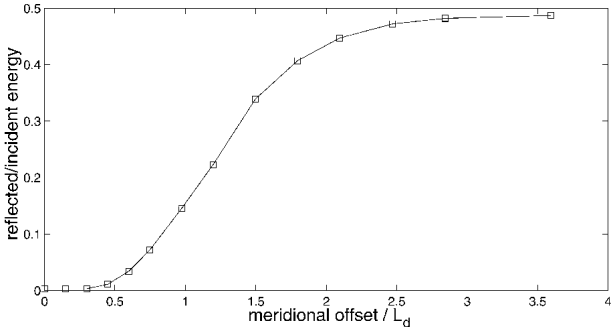

FIG. 3. Energy reflected into eastward-propagating Kelvin waves as a function of gap offset from the equator (normalized by the incident energy flux).

tial thickness anomaly. This was done so that the initial anomaly would fit entirely within the model domain. These calculations were sufficiently nondispersive that the initial structure of the thickness anomaly was maintained as it propagated westward, and higher-frequency modes were not excited to a significant degree.

The fraction of the incident energy flux that continues to propagate westward in the western basin is shown in Fig. 4 as a function of the wave frequency. The lowest-frequency waves transmit 60% of the incident energy, while the highest-frequency waves transmit only 30% of the incident energy. There is very little change in the percent of transmitted energy for frequencies below approximately $0.25\omega_{\max}$ in the model. This compares reasonably well to the theory developed in the appendix (indicated by the dashed line in Fig. 4). In all cases, very little energy is reflected into eastward-propagating Kelvin waves.

b. Examples with two gaps

A series of calculations have been carried out with one gap located on the equator and a second gap of 75-km width shifted systematically northward from the equator. The frequency of the incident wave in these cases is 2.5×10^{-7} s^{-1} and the model is initialized with a one-half wavelength anomaly to the east of the barrier. The total energy flux through the gaps after the anomaly has fully propagated into the western basin is shown in Fig. 5 as a function of the distance of the second gap from the equator. If the second gap is located within a deformation radius of the equator, there is very little effect on the energy flux into the western basin compared to the single gap case. However, the energy transmission increases to as much as 75% for islands greater than the deformation radius with the maximum transmission found for a second gap placed approximately 3 times the deformation radius off the equator. An additional increase to approximately 83% is found when a third gap is placed $3L_d$ to the south of the equator. This enhanced transmission is still noticeable, even when the second gap is located 10 deformation radii off the equator.

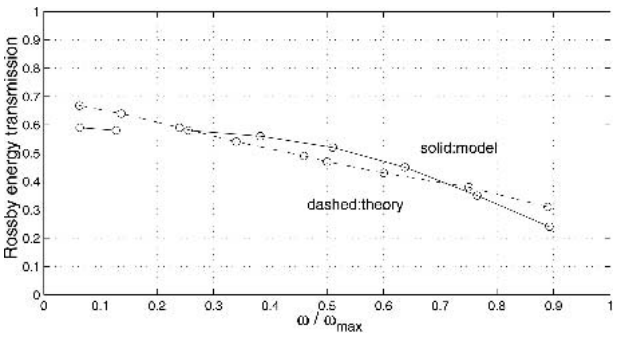

FIG. 4. Energy transmission into the western basin (normalized by the incident energy flux) as a function of the wave frequency. The solid line is diagnosed from a series of numerical integrations; the dashed line is the theory presented in the appendix.

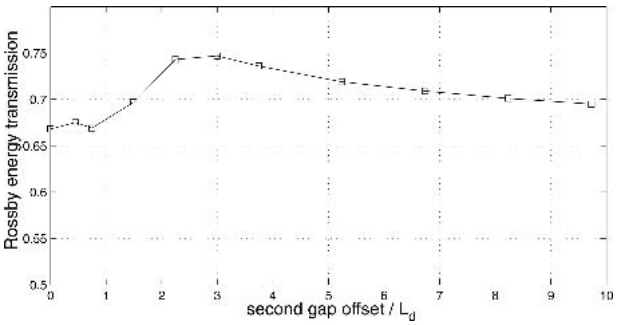

FIG. 5. Energy transmission into the western basin (normalized by the incident energy flux) as a function of the offset of a second gap from the equator based on numerical integrations.

This behavior is reminiscent of the midlatitude influence of adding a second gap to a western boundary, although the net effect is not as dramatic. Simple analytic solutions to the circulation integral based on quasi-geostrophic dynamics, as used in midlatitudes, are not available near the equator. However, it is evident from the circulation around the island that a similar constraint is at play here. This is demonstrated by the height and velocity (every fourth point) fields as the negative thickness anomaly of a Rossby wave is passing through the barrier for a case with the poleward gap placed $3L_d$ away from the equator (Fig. 6). There exists a stagnation point just north of the midpoint of the eastern side of the island. To the north of this point, the flow is directed toward the northern gap. The presence of the northern gap limits the extent of the poleward propagation of the thickness anomaly on the western side of the barrier and results in transport between the two basins. The flow through the gap is essentially geostrophic, and so is balanced by a pressure drop between the northern tip of the island and the barrier to the north. This circulation around the island results in a decrease in the pressure on the eastern side of the island as compared with the pressure in the absence of the second gap (see southern half of the reflecting Rossby wave). The amount of incident energy that is reflected into short Rossby waves on the eastern side of the island is thus reduced in comparison with the single-gap case because the boundary condition that gives rise to the reflected waves has been relaxed. In all of the cases with a gap on the equator, very little energy is reflected into eastward-propagating Kelvin waves, and so the energy that does not go into reflected short Rossby waves is fluxed into the western basin and radiated westward.

Analytic treatments of the complex topography and multiple islands composing the Indonesian Throughflow have often simplified the governing equations by making use of the low frequency limit, for which the meridional velocity approaches zero (DuPC, C91). This allows considerable simplification, not only of the gov-

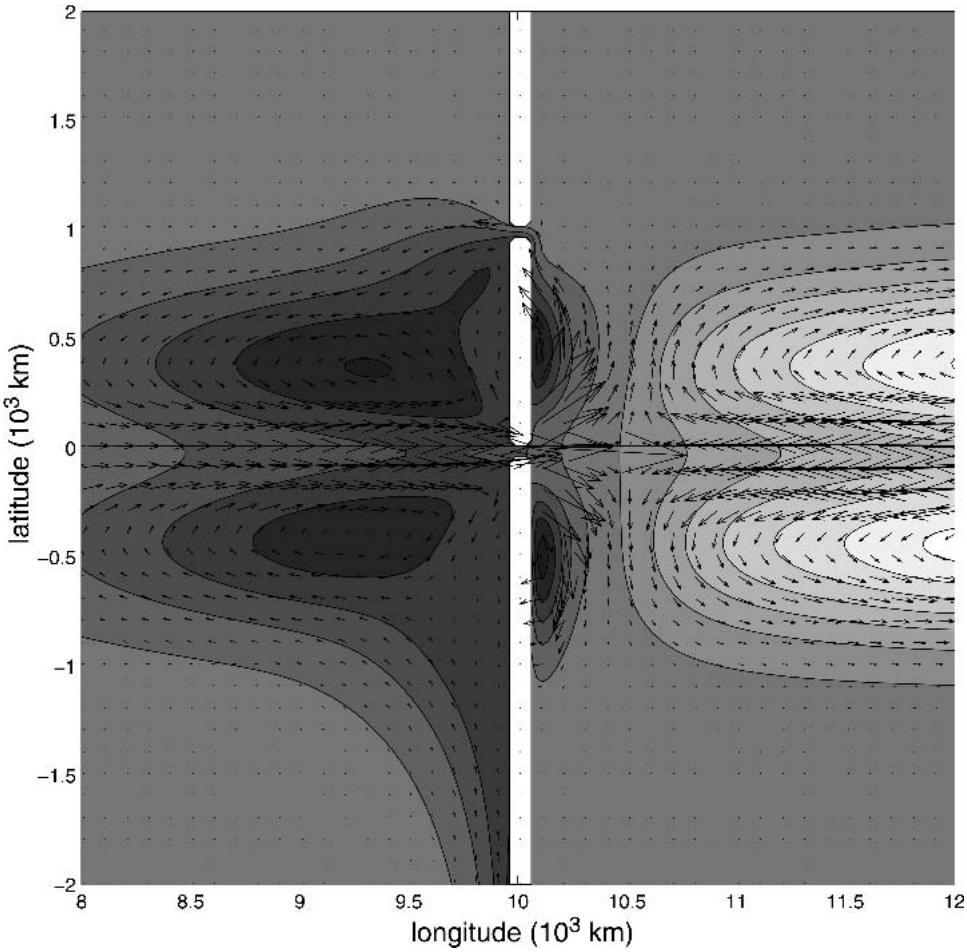

FIG. 6. Layer thickness anomaly (contours) and velocity vectors (every fourth grid point) for a case with two gaps, the poleward gap being located $3L_d$ away from the equator.

erning equations (for which the meridional velocity may be set to zero) but also of the geometry. In this limit, islands contained entirely within the latitude limits of other islands located to the east have no influence on the circulation or energy transmission and do not need to be considered. This is because the zonal jets extending to the west of the easternmost islands must remain purely zonal and, hence, cannot interact with islands located at latitudes not occupied by the jets.

We have tested the applicability of this low-frequency limit by placing a second island to the west of the island defined by the two gaps in the barrier, as shown in Fig. 7. The frequency of this Rossby wave is 2×10^{-7} s^{-1}, or approximately 10% of the maximum frequency, with a wavelength of 23 360 km. The wave clearly interacts with the second island located to the west, reducing the amplitude of the transmitted wave in comparison with the case without the shadow island. Recall that in the absence of the second island, the transmission in the Northern Hemisphere is greater than that in the Southern Hemisphere. The zonal energy flux after 250 days for cases with and without the shadow island are shown in Fig. 8. The thickness anomaly has propagated past the islands by this time, but the energy flux decays westward because of the trapped modes along the western side of the barriers. The two calculations are very similar to the east of the western island, but the zonal energy flux drops rapidly by approximately 10% when the second island is encountered. This decrease in energy flux is similar for cases in which the second island is located 500 and 300 km to the west of the eastern island. Similar reductions in the energy flux are also found for cases with $\omega/\omega_{\max} = 0.15, 0.25, 0.375$, so this result does not appear to be very sensitive to the frequency of the incident wave. This meridional spreading is not due to numerical diffusion but is instead due to dispersion ignored in the long wave theory. The width of a diffusive boundary layer grows to the west as $\delta_m^{.75}x^{.25}$, where $\delta_m = (A_\nu/\beta)^{1/3}$ is the Munk layer thickness and x is distance westward. For the lateral viscosity used here, the boundary layer would grow to only 40-km width over 1000-km separa-

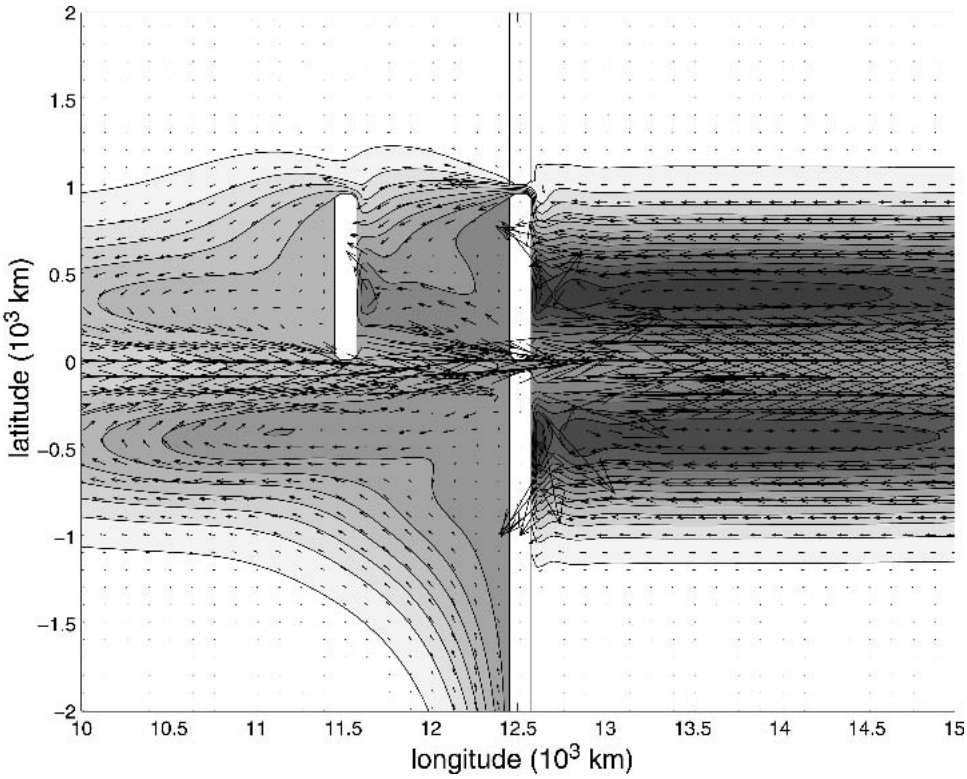

FIG. 7. Layer thickness anomaly (contours) and velocity vectors (every fourth grid point) for a case with a second island located directly to the west of the primary island.

tion between the islands. This effect is entirely negligible over the 1000-km meridional extent of the island.

Even though the meridional velocity becomes very small as the wavelength of the wave increases and the frequency decreases, scaling as $v/u = O(2\pi L_d/\lambda)$, it still remains nonzero. It is the integral effect of the weak meridional velocity over the very long period of the wave that dictates the net effect of the island. This meridional redistribution of mass induces a zonal flow that interacts with the shadowed island. The zonal component of this velocity must satisfy the no-normal flow condition on the island, and thus requires the reflection of short Rossby waves and dissipation.

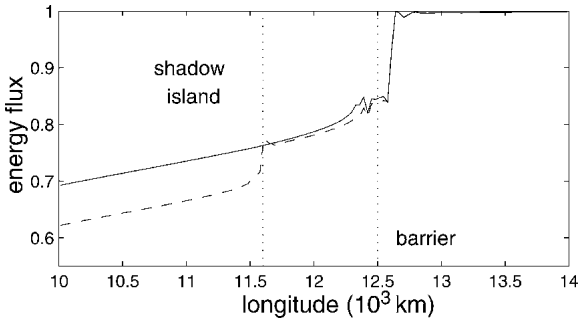

FIG. 8. Zonal energy flux (normalized by the westward Rossby wave energy flux) as a function of longitude for the calculations with a single island (solid line) and with a shadow island (dashed line). The positions of the islands are indicated by the dotted lines.

c. *Application to the Indonesian Throughflow*

Here we apply the shallow-water model to the reflection and transmission of equatorial Rossby waves generated by wind anomalies on the equator. This is motivated by the delayed oscillator mechanism of ENSO in which the eastward propagation of warm waters induces wind stress anomalies, which in turn generate a cold Rossby wave that propagates toward the western boundary. A key aspect of the oscillator is the reflection of this Rossby wave into an eastward-propagating cold Kelvin wave, which causes the decay of the anomalous wind forcing when the wave reaches the central Pacific. The calculations in this section are initialized with a motionless ocean and forced by applying a zonal wind stress in the central Pacific, centered on the equator with a Gaussian decay in both the zonal and meridional directions and sinusoidal variation in time:

$$\tau = \tau_0 \sin(2\pi t/P) e^{-[(x-x_0)/L_x]^2-[(y-y_0)/L_y]^2}, \quad 0 < t < P/2, \quad \text{and} \tag{3}$$

$$\tau = 0, \quad t > P/2. \tag{4}$$

The wind is centered at $x_0 = 15\,000$ km and $y_0 = 0.0$ with zonal decay scale of $L_x = 1000$ km. The meridional decay scale L_y will be varied between 100 and 700 km. Although ENSO events occur on average every 3–4 years, the anomalous wind events in the central Pacific associated with ENSO have a duration of closer to 1 year. The period of the wind forcing P will be varied between 6 and 48 months. The wind forcing is active for one-half period and the model is run for 360 days after the wind forcing is turned off. This is to allow the thickness anomalies generated in the basin interior to propagate to the west and interact with the islands. It takes a first-mode baroclinic Rossby wave approximately 165 days to propagate from the forcing region to the western boundary, and so this allows ample time for the wave propagation and reflection to complete its cycle.

The islands for this calculation are defined by the 200-m isobath, derived from the Smith and Sandwell (1997) bottom topography, averaged onto a ⅙° grid (Fig. 9). The model is integrated in a domain that extends 30 000 km in the zonal direction and 4700 km in the meridional direction. There are sponge layers in the easternmost 5000 km and westernmost 2500 km where the layer thickness is restored toward zero with a time scale of 30 days. This prohibits reflection of waves from the model boundaries and allows us to attribute any wave reflection to the islands. The region of wind forcing is indicated near $x = 15\,000$ km in Fig. 9 by the white contours.

The thickness anomaly for the case with $L_y = 400$ km and $P = 720$ days is shown in Fig. 9 after 280 days. The wind forcing generates a negative thickness anomaly that propagates westward as a combination of first-mode and third-mode Rossby waves (for a meridional decay scale greater than the deformation radius, most of the energy is in the first mode). This negative thickness anomaly is interacting with the islands to the west and penetrating into the Indian Ocean. The wind forcing also generates a positive thickness anomaly that propagates to the east as a Kelvin wave. To distinguish between eastward-propagating Kelvin waves generated from reflection at the islands and those generated from the wind forcing, this calculation was compared with a calculation that was identical except that there were no landmasses to the west. The difference between the energy flux in each of these calculations must be due to reflection and dissipation resulting from the coastlines. The energy flux as a function of time and longitude is shown for these two cases in Fig. 10. The calculation without islands shows eastward (dashed contours) and westward (solid contours) energy propagation away from the forcing region. The westward energy flux decays near the western boundary because of the sponge region. There is no significant reflection from either the western or eastern boundaries of the model domain. The energy flux for the case with islands (Fig. 10b) shows two primary differences. The westward energy flux does not penetrate to the west of the islands. Abrupt decreases are seen at the island longitudes. There is now also a second pulse of eastward energy flux that can be traced to the interaction of the westward-propagating Rossby waves with the islands. This is clearly offset in time from the initial Kelvin wave directly forced by the wind.

The total amount of incident energy reflected into eastward propagating Kelvin waves is 23%. This was calculated as the difference in the energy flux in these two model calculations just to the east of the islands ($x = 8000$ km), normalized by the westward energy flux for the case with no islands. The energy transmitted into the Indian Ocean is only 10% of the incident energy flux (this is very close to that predicted by C91). The remainder of the energy is dissipated along the eastern boundaries of the islands.

The energy reflection found here is significantly less than the approximately 35% efficiency predicted by the theories of C91 and DuPC. The actual geography of the islands near the equator in the western Pacific Ocean is quite complex. The theories of C91 and DuPC assume that the islands are thin and aligned in a meridional

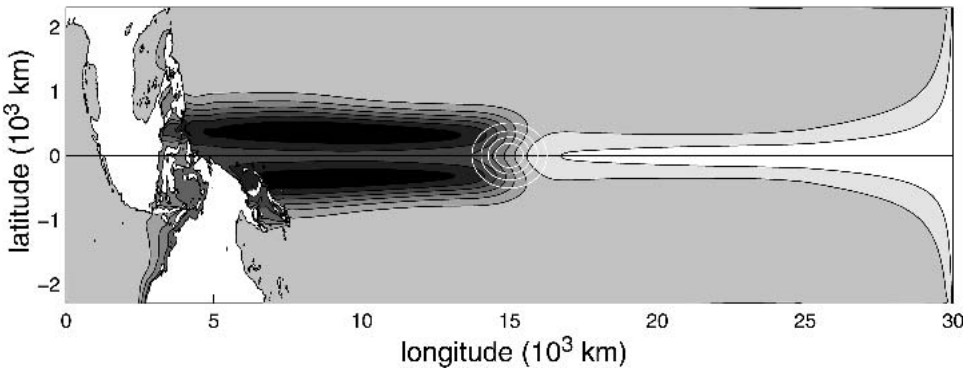

FIG. 9. Layer thickness anomaly generated by anomalous wind forcing in the central Pacific (white contours near $x = 15\,000$ km). Rossby waves propagate the signal westward while a Kelvin wave propagates the signal eastward.

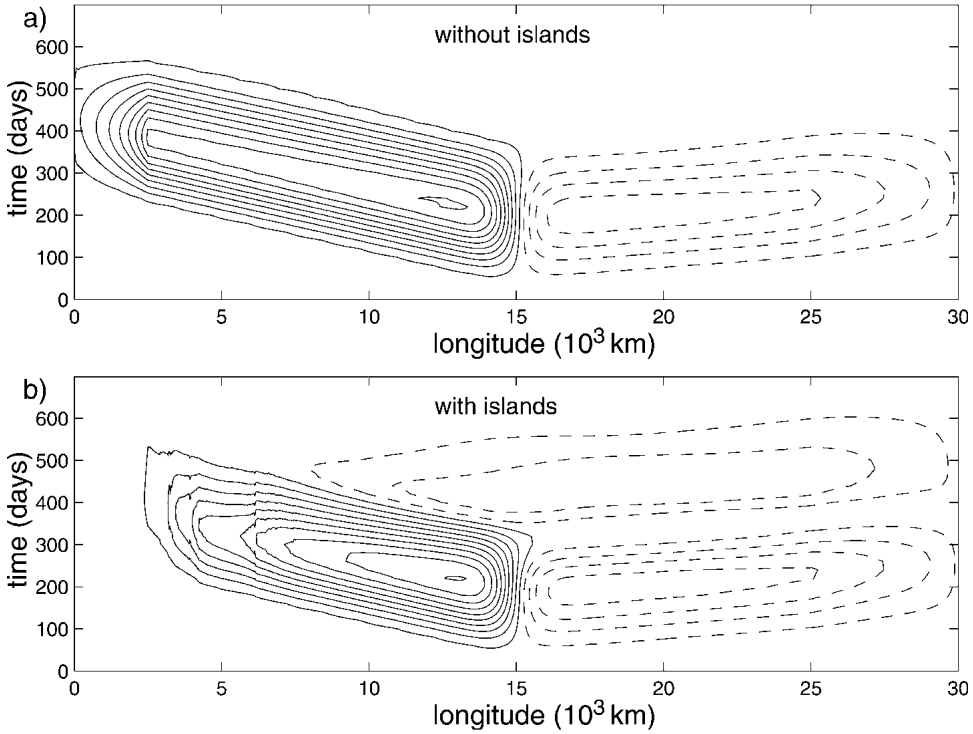

FIG. 10. Energy flux as a function of longitude and time (solid contours westward, dashed eastward) for (a) case with no islands and (b) case with islands represented by the 200-m isobath in the western Pacific.

direction. We did a wind-forced calculation using seven meridional islands to represent the major landmasses, as in C91. The results from this case are very similar to the realistic topography case, producing 23% reflection and 6% transmission (not shown). This suggests that the much lower reflection found here is not due to the different coastline orientation.

A series of calculations was carried out in which the duration and meridional scale of the wind forcing was varied. Each of these runs was integrated for 360 days after the forcing ceased, and the reflected energy was calculated by comparing twin runs with and without islands, as in Fig. 10. The previous case used forcing typical of ENSO events and is located near the center of Fig. 11 (1-yr forcing, $L_y/L_d = 1.2$). The reflected energy increases with increasing meridional length scale and with longer forcing. For the longest forcing duration (2 yr) and largest meridional decay scale (700 km), the reflected energy is 37%, very close to that predicted by C91 and DuPC. Events with smaller meridional length scales produce very little reflection regardless of the duration of the forcing event. This is because most of the energy at these smaller scales goes into mode-3 Rossby waves, which reflect much less energy into Kelvin waves at all frequencies (Clarke 1983). The duration of the forcing becomes more important as the meridional scale of the winds exceeds the deformation radius, the scale at which the energy is predominantly carried by the mode-1 Rossby wave. The amount of energy transmitted into the Indian Ocean varies between 5% for the smallest meridional forcing scale and 10% for the largest meridional forcing scale with very little dependence on the duration of forcing (not shown).

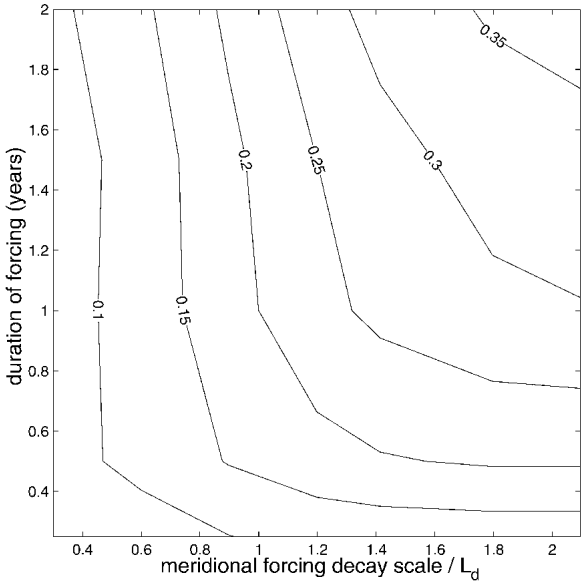

FIG. 11. Reflected energy (normalized by the incident energy flux) as a function of the duration of forcing and the meridional Gaussian decay scale.

3. Summary

Numerical model calculations have shown that low-frequency equatorial Rossby waves incident upon a western boundary with one or more narrow gaps near the equator reflect only a small fraction of the incident energy into eastward-propagating Kelvin waves. Basic principles are first developed using idealized configurations including single gaps in the western boundary, two gaps, and two islands. Very little energy is reflected into Kelvin waves provided that at least one gap is located within a deformation radius of the equator. Because of circulation integral constraints around an island, the introduction of a second gap enhances the transmission into the western basin. It is also found that wave dispersion, even in the low-frequency limit, remains important and results in reduced energy transmission in the presence of shadowed or blocked islands.

The amount of reflected energy for idealized and more realistic representations of the actual geometry of the western Pacific and Indonesian Throughflow forced by wind stress in the midocean depends on the meridional length scale and duration of the forcing events. For winds that persist for 2 yr with a meridional length scale of 700 km, we find reflection that is very close to that predicted by the low-frequency theories of Clarke (1991) and Du Penhoat and Cane (1991). For parameters more typical of ENSO (1 yr, 400–700 km), we find 23%–30% reflection. Winds with meridional length scales less than the deformation radius produce only weak reflection over all time scales.

The efficiency with which incident waves reflect energy into Kelvin waves bears on the ability of this process to play an active role in sustaining low-frequency El Niño oscillations in the equatorial Pacific Ocean. The reflection efficiency that we find for ENSO parameters is between the 14% efficiency estimated by Battisti and Hirst (1989) to be required to sustain low-frequency oscillations and the 35% predicted (and found) for very low frequency and large-scale waves. Thus, our results imply that this mechanism may be an effective trigger for the initiation or decay of El Niño events, provided that the winds persist for long enough. Short wind events or winds with small meridional scales do not produce strong reflection. This prompts the question of whether it is coincidental that the length and time scales of ENSO wind stress anomalies coincide with the forcing at which westward-propagating energy is able to be effectively reflected into eastward-propagating Kelvin waves.

Acknowledgments. The authors thank Allan Clarke, Ted Durland, and Lisan Yu for their thoughtful comments and suggestions. This work was supported by the Office of Naval Research under Grant N00014-03-1-0338 (MAS) and by the National Science Foundation under Grants OCE-0240978 (MAS) and OCE-9901654 (JP).

APPENDIX

Theory for the Transmission of Wave Energy through a Narrow Equatorial Gap

Our theoretical development is based on the results of a fundamental numerical experiment in which an equatorial Kelvin wave, traveling eastward, impinges on a barrier with a single, narrow gap placed at the equator (Fig. 2). The finding that essentially all of the incident Kelvin wave energy is able to penetrate through the gap and into the eastern basin leads us to develop a theory for the transmission from the eastern basin into the western basin in which the reflected Kelvin mode is absent. In the low-frequency limit of interest, the reflected short Rossby waves carry negligible mass, and so we take as our central hypothesis that all the mass in the incident wave must be fluxed through the gap.

Consider the incident wave to be a first-mode long Rossby wave. In this case the velocity and height fields are

$$v_i = A_i e^{i(k_i x - \sigma t)} \psi_J(\eta), \tag{A1a}$$

$$u_i = iA_i \left\{ \frac{(J/2)^{1/2}}{(\sigma + k_J)} \psi_{J-1} + \frac{[(J+1)/2]^{1/2}}{(\sigma - k_J)} \psi_{J+1} \right\}, \quad \text{and} \tag{A1b}$$

$$h_i = iA_i \left[-\frac{1}{\sigma + k_J} \left(\frac{J}{2} \right)^{1/2} \psi_{J-1} + \frac{1}{\sigma - k_J} \left(\frac{J+1}{2} \right)^{1/2} \psi_{J+1} \right], \tag{A1c}$$

where $J = 1$.

Here, the usual equatorial scaling is used. Lengths have been scaled with the equatorial deformation radius, $(c/\beta)^{1/2}$, and so η is the y variable so scaled. The frequency σ is dimensional frequency ω scaled by $(\beta c)^{1/2}$ where c is the Kelvin wave speed. The ψ_J are the standard Hermite functions. The wavenumber is also scaled with the deformation radius. In (A1) we take $J = 1$ for the case under discussion. The wavenumber for the long Rossby wave is

$$k_J = -\frac{1}{2\sigma} + \frac{1}{2}[(\sigma^{-1} - 2\sigma)^2 - 8J]^{1/2}. \tag{A2}$$

The amplitude of the integrated mass flux in the incident wave for which $J = 1$ is

$$U_g = -2i\pi^{1/4} \frac{\sigma}{\sigma^2 - k_1^2} A_i. \tag{A3}$$

The basic hypothesis that all the mass flux of the incident wave squeezes through the gap leads to the boundary condition for the transmitted motion in the western basin. With the barrier at $x = 0$, we assume that the narrow gap provides a delta function mass source

that drives the motion of the western basin. Thus, the boundary condition for the transmitted field is, using the orthogonality properties of the Hermite functions,

$$u_T = U_g \delta(\eta) e^{i\sigma t} = U_g \sum_{j=0}^{J_{\max}} \psi_j(0)\psi_j(\eta) e^{i\sigma t}. \quad \text{(A4)}$$

The transmitted wave has a zonal velocity,

$$u_T = i \sum_{j=0}^{J_{\max}} A_T(j) \left\{ \frac{(j/2)^{1/2}}{(\sigma + k_j)} \psi_{j-1} + \frac{[(j+1)/2]^{1/2}}{(\sigma - k_j)} \psi_{j+1} \right\} e^{i(k_j x - \sigma t)}, \quad \text{(A5)}$$

where the wavenumbers k_j are given by (A2) with J replaced by the running index j. The real part of the above expression is understood. The sums in (A4) and (A5) are truncated at a maximum value $J_{\max}$. In the calculations $J_{\max}$ of 260 was found to be sufficient for a calculation of the energy flux. Raising the value further produced no alteration. Equating the two equations yields a recursive relation for the transmitted wave amplitudes; by symmetry all the amplitudes for j even are zero, and

$$A_T(1) = -iU_g \frac{2^{1/2}(\sigma + k_1)}{\pi^{1/4}}. \quad \text{(A6a)}$$

For $j > 1$,

$$A_T(j) = -A_T(j-2)\left(\frac{j-1}{j}\right)^{1/2} \frac{\sigma + k_j}{\sigma - k_{j-2}} - iU_g\left(\frac{2}{j}\right)^{1/2} (\sigma + k_j)\psi_{j-1}(0). \quad \text{(A6b)}$$

Once the amplitudes are determined, the energy flux of the transmitted wave can be determined. Since the variable h, the thickness anomaly, is equivalent to the pressure field, the energy flux in the x direction is simply

$$F = \int_{-\infty}^{\infty} h_T u_T \, d\eta \quad \text{(A7)}$$

and can easily be determined. When integrated in y and averaged over the period of the wave, this flux can be written

$$F_{\text{trans}} = \sum_{j=1}^{J'} \frac{|A_T(j)|^2}{4} \left[\frac{j+1}{(\sigma - k_j)^2} - \frac{j}{(\sigma + k_j)^2} \right], \quad \text{(A8)}$$

where J' is the largest value of j corresponding to a real k_j. The ratio of the transmitted energy to the same quantity in the incident wave with $J = 1$ is plotted as the dashed line in Fig. 4. The agreement between the theory and the direct numerical calculation is quite good.

REFERENCES

Battisti, D. S., 1988: Dynamics and thermodynamics of a warming event in a coupled tropical atmosphere–ocean model. *J. Atmos. Sci.,* **45,** 2889–2919.

——, and A. C. Hirst, 1989: Interannual variability in a tropical atmosphere ocean model: Influence of the basic state, ocean geometry, and nonlinearity. *J. Atmos. Sci.,* **46,** 1687–1712.

Boulanger, J.-P., S. Cravatte, and C. Menkes, 2003: Reflected and locally wind-forced interannual equatorial Kelvin waves in the western Pacific Ocean. *J. Geophys. Res.,* **108,** 3311, doi:10.1029/2002JC001760

Clarke, A. J., 1983: The reflection of equatorial waves from ocean boundaries. *J. Phys. Oceanogr.,* **13,** 1193–1207.

——, 1991: On the reflection and transmission of low-frequency energy at the irregular Pacific Ocean boundary. *J. Geophys. Res.,* **96,** 3289–3305.

Du Penhoat, Y., and M. Cane, 1991: Effect of low-latitude western boundary gaps on the reflection of equatorial motions. *J. Geophys. Res.,* **96,** 3307–3322.

Harrison, D. E., and G. A. Vecchi, 1999: On the termination of El Nino. *Geophys. Res. Lett.,* **26,** 1593–1596.

Li, B., and A. J. Clarke, 1994: An examination of some ENSO mechanisms using interannual sea level at the eastern and western equatorial boundaries and the zonally averaged equatorial wind. *J. Phys. Oceanogr.,* **24,** 681–690.

McKee, W. D., 1972: Scattering of Rossby waves by partial barriers. *Geophys. Fluid Dyn.,* **4,** 83–89.

Pedlosky, J., 2000: The transmission of Rossby waves through basin barriers. *J. Phys. Oceanogr.,* **30,** 495–511.

——, and M. A. Spall, 1999: Rossby normal modes in basins with barriers. *J. Phys. Oceanogr.,* **29,** 2332–2349.

Potemra, J. T., 2001: Contribution of equatorial Pacific winds to southern tropical Indian Ocean Rossby waves. *J. Geophys. Res.,* **106,** 2407–2422.

Schopf, P. S., and M. J. Suarez, 1988: Vacillations in a coupled ocean–atmosphere model. *J. Atmos. Sci.,* **45,** 549–566.

Smith, W. H. F., and D. T. Sandwell, 1997: Global seafloor topography from satellite altimetry and ship depth soundings. *Science,* **277,** 1957–1962.

Verschell, M. A., J. C. Kindle, and J. J. O'Brien, 1995: Effects of Indo–Pacific throughflow on the upper tropical Pacific and Indian Oceans. *J. Geophys. Res.,* **100,** 18 409–18 420.

Zang, X., L.-L. Fu, and C. Wunsch, 2002: Observed reflectivity of the western boundary of the equatorial Pacific Ocean. *J. Geophys. Res.,* **107,** 3150, doi:1029/2000JC000719.